PULMONARY MACROPHAGES: PHENOMENA ASSOCIATED WITH THE PARTICLE "OVERLOAD" CONDITION

B.E. Lehnert[1], R.J. Sebring[1], and G. Oberdörster[2]
[1]Los Alamos National Laboratory, Los Alamos, NM, U.S.A., and the
[2]University of Rochester, Rochester, NY, U.S.A.

ABSTRACT

Numerous lines of evidence support the generalization that alveolar macrophage (AM)-mediated particle clearance, or the transport of particle-containing AM from the alveoli out of the lung via the mucociliary apparatus, is a prominent mechanism that determines the pulmonary retention characteristics of relatively insoluble particles. Several studies have also shown that the alveolar deposition of excessive burdens of particles with even low intrinsic cytotoxicity can result in impairments of the AM-mediated particle clearance mechanism and the development of pathologic disorders including pulmonary fibrosis and lung cancer, at least in the lungs of rats. In this report, we briefly review evidence consistent with the idea that the high volumetric loads of particles contained in AM during "particle overload" conditions underlies their inabilities to translocate from the lung. However, it remains possible that other mechanisms may also contribute to retardations in the clearance of particles from the lung during particle overload. Using a condition of particle overload brought about by subchronic exposure of rats to ultra-fine titanium dioxide as an experimental model, we have obtained ultrastructural and other evidence that indicates an association between particle overload and: 1) the occurrence of aggregates of particle-containing AM in alveoli, 2) Type II cell hyperplasia in alveoli that contain the AM aggregates, 3) a loss in patent pores of Kohn in alveoli that contain the AM aggregates and show Type II cell hyperplasia, 4) the interstitialization of particles at the sites where these phenomena collectively occur, and 5) the development of fibrosis in alveolar regions where particle interstitialization occurs. The loss of pores of Kohn in the alveoli that contain aggregates of particle laden AM is of particular interest. In addition to the liklihood that these interalveolar pores normally serve as passageways through which AM may migrate to neighboring alveoli as they perform their function of phagocytizing particles that have deposited on the alveolar surface, it remains possible that the pores of Kohn also serve as short cut pathways for AM to reach the mucociliary apparatus from more distal alveoli.

INTRODUCTION

The lung's population of alveolar macrophages (AM) are fundamentally involved in mediating the removal of particles from the lung by way of the conducting airways. Circumstantial evidence for such AM-mediated particle clearance comes from numerous sources, including observations of particle-containing macrophages on airway surfaces at times well after the particles were deposited in the lungs (e.g., Ferin, 1971), inferential extensions of experimental results that have shown that the bulk of particles retained in the lung are associated with AM over the course of alveolar phase clearance (e.g., Lehnert and Morrow, 1985), findings that insoluble particles that are removed from the lung can be quantitatively accounted for in the gastrointestinal tract and feces (Gibb and Morrow, 1962), and, more recently, the observation that the distributions of particles in macrophages on the surfaces of the conducting airways are virtually identical to those found in more peripheral AM over the course of alveolar phase clearance (Lehnert et al., 1990). Although various mechanisms have been proposed concerning how AM ultimately translocate from the alveoli with their particulate burdens and gain access to the mucociliary apparatus for cephalad transport have been offered (for review, see Lehnert, 1992) evidence in support of these is scant or lacking. Thus, the mechanistic bases of AM-mediated lung clearance remain to be elucidated.

Several animal studies have demonstrated that alveolar phase clearance becomes diminished following the excessive deposition of a variety of relatively insoluble materials, including carbon black, titanium dioxide, particulate diesel exhaust, and even polystyrene microspheres (Wolff et al., 1987; Lee et al., 1986; Lehnert, 1990). Of particular concern is the association between excessive lung burden-induced compromises in lung clearance, i.e., "particle overload", and the development of pulmonary fibrosis and lung tumors that occurs with particles that might otherwise be viewed as being generally innocuous (e.g., Lee et al., 1986). Accordingly, numerous investigators have become increasingly interested in elucidating the mechanism(s) that underlie particle overload, with emphasis being placed on the effects of particle overload on AM-mediated particle clearance.

In 1988, Morrow postulated that the failure of removal of AM from the lung in a condition of particle overload is due to their containment of high volumetric loads of particles (Morrow, 1988). According to his hypothesis, the removal of an AM from the lung via the conducting airways virtually ceases when the phagocytized volumetric burden of particles in the AM reaches ~600 μM^3, or ~60% of a normal AM's volume. Experimental support for this possibility has mounted. For example, Oberdörster and colleagues (1992) published a report in which they examined the alveolar clearance rates of

low numbers of 3.3 μM diam. and 10.3 μM diam. radiolabeled, polystyrene particles that had been deposited in the lungs of rats. They found that the larger particles, which were approximately equivalent to 60% of the normal volume of AM, were persistently retained in the lungs with a half-time of ~1000 days, whereas the smaller particles were readily removed from the lung with a 60-70 day half-time. In a similar, earlier study, Snipes and Clem (1981) also reported that the retention half-times following the instillation of 9 and 15 μM diam. microspheres into the lungs of rats were ~580 days and virtually infinite, respectively. Along the same line, Lehnert (1990a) also found that decreases in alveolar phase clearance following the deposition of high numbers of polystyrene microspheres (2 μM diam.) in rat lungs could be attributed to the failure of clearance of AM whose volumetric burdens of the particles were $\geq$ 60% of the normal cellular volume of AM.

Whether other mechanisms in addition to a volumetric overloading of AM may contribute to diminished alveolar clearance rates seen in particle overloading conditions have yet to be examined. It is known that several anatomical changes accompany conditions of particle overload. For example, in the aforementioned study by Lehnert in which particle overloading was brought about by the intratracheal instillation of high numbers of microspheres, phenomena that were associated with the overloaded condition included the focal occurrence of aggregates of particle-laden AM in the alveoli, the appearance of Type II cell hyperplasia in alveoli that contained the AM aggregates, and the interstitialization of particles in alveolar regions where the AM aggregates and Type II cell hyperplasia were present (Lehnert, 1990a, Lehnert, 1990b).

In the present study, we set out to further investigate anatomical changes that occur in the lung during a condition of particle overload brought about by subchronically exposing rats to aerosolized ultra-fine titanium dioxide (TiO_2). As will be shown herein, the deposition of excessive amounts of the TiO_2 resulted in markedly impaired lung clearance, which was accompanied by the focal occurrence of particle-laden AM and Type II cell hyperplasia and septal wall thickening in the alveoli that contained the aggregated AM. Of potential relevance to AM mediated particle clearance, we also report that such septal thickening results in a loss of patent pores of Kohn. Finally, we show evidence that particles are extensively interstitialized in alveolar regions where these phenomena collectively occur, and that fibrotic processes occur at sites where interstitialized particles are contained in interstitial macrophages.

MATERIALS and METHODS

Animals and Aerosol Exposures: Male Fischer 344 rats (specific-pathogen-free, 240-260 g) were exposed to aerosolized fine titanium dioxide (TiO_2-F, 0.25 μM geo. dia., anatase, Fisher Scientific, Springfield, NJ) or ultra-fine TiO_2 (TiO_2-D, 0.021 μM geo. dia., Degussa A.G. Frankfort am Main, FRG) in whole body chambers using horizontal laminar flow in conjunction with a Wright Dust Feed generator (Ferin et al., 1991). Both types of the TiO_2 were delivered to different groups rats at average concentrations of ~24 mg/M^3 for six hours/day, five days per week, for a total of 12 weeks. The MMAD and σ_g of the TiO_2-F and TiO_2-D were 0.71 μM ± 1.9 and 0.78 μM ± 1.7, respectively. A control group of rats was exposed to filtered air only. Two animals from each exposure group were killed by lethal injections of pentabarbital sodium on days 30 and 60 after the onset of the exposures, one day after the last day (day 90) of exposure, and as of six months after cessation of the exposures.

Lung Fixation and Processing: This report specifically focused on the anatomical changes we observed with the lungs from rat exposed to the TiO_2-D. The lungs were filled *in situ* with glutaraldehyde in Sorenson's phosphate buffer at a constant fixation pressure of 25 cm H_2O and further fixed after excision. Three slices, one near the top, the middle and the bottom, were cut perpendicular to the long axis of the left lobe of each lung and further cut into smaller two-three mM cubes. For this study, only samples taken from the middle slices were used. The lung pieces were post-fixed in 1% OsO_4, followed by 2% uranyl acetate, and then dehydrated in graded concentrations of ethanol and 100% propylene oxide. The samples were then infiltrated with LX110 resin and cured. Several 2 μM thick plastic sections, approximately 2-3 mM in dimension, were cut from each tissue block on an ultramicrotome (LKB Bromma, Sweden) using a glass knife. The sections were subsequently dried onto a glass microscope slide, stained intensely with toluidine blue, and covered slipped in Aqua-Poly/Mount (Polysciences Cat. # 18606). Thin sections (500-700 Angstroms thick) were cut with a diamond knife, mounted on 200 mesh copper grids, and stained with uranyl acetate and lead citrate. The samples were visualized and photographed using a Philips transmission electron microscope.

Overview of Tissue Analyses: Two types of indexes (to be described), a mean linear intercept value and a area to perimeter ratio (A/P), were used on the same light microscopic fields to measure alveolar wall thickening, due at least in part to the Type II cell hyperplasia

that generally accompanied the focal accumulation of TiO_2-laden AM as early as 60 days after the onset of exposure to TiO_2-D, Figures 1A and 1B. After these measurements, the number of pores was determined by counting the number of pores in the alveolar septal walls within a measurement field.

Two different tissue sampling methods were used. In the initial phase of the study, we randomly selected tissue blocks from each animal's lung for sectioning and analysis. It became apparent as these analyses proceeded that the lung areas demonstrating septal thickening were highly localized, Figure 2, and that they appeared to correlate with aggregates of TiO_2-containing AM. Within a few alveoli outside of these focal regions, the alveolar septum often showed little or no thickening, and the number of pores subjectively appeared to be "normal". Since these foci represented a relatively small volume of the total tissue, it became evident that any random sampling approach would require extensive sampling to statistically represent them.

Based on the results from the random sampling phase of our study, we continued our investigation using a biased, non-random, selection strategy. The tissue blocks from three and six month post-exposure to TiO_2-D samples where selected and faced so that subsequent sections from a tissue block included at least one focal region. The foci were easily visible in the tissue blocks under a low power dissecting microscope and appeared as "white spots" because of the large accumulation of TiO_2 in the AM aggregates. A section selected in this fashion typically contained 1 or 2 distinct foci that accounted for up to about 20% of the lung section area. The focal regions were then targeted for the measurement by intentionally centering them within a measurement field. Once the fields containing these foci were measured, all other measurable parenchyma on the same section was also measured, regardless of the amount of septal thickening present. Thus, the values obtained from this part of the study likely *underestimate* the structural endpoints we measured.

Tissue Area/Perimeter Ratios and Mean Linear Intercepts. Each microscopic lung field containing 30-70 alveolar profiles was digitized as a 64 gray level, 512 x 512 pixel resolution image (Figure 3A) using a video digitization and image analysis system that has been described in detail elsewhere (Sebring and Lehnert 1992). The digitized image and the real time video image of the same field were displayed side by side on two separate B/W video monitors. A binary image representing the lung parenchyma to be measured (Figure 3C) was generated from the digitized gray image by selecting a range of gray values from the total gray values in the original digitized image (Figure 3B) i.e., gray level thresholding (Russ and Russ, 1984). The binary image was then edited to

remove non-parenchymal features from the image, see Figures 4A and 4B. This was accomplished by visually analyzing the live B/W gray image at higher magnification to determine which features in the lower magnification binary image were to be removed. All fine parenchyma on a section was first systematically analyzed to exclude any alveoli within three alveoli of either the visceral pleural or major blood vessels or conducting airways. Thereafter, the field of was further edited to exclude AM and intra-alveolar debris, as well as blood vessels and terminal bronchioles greater than 40 μM in diameter. Once the binary image was so edited, it was further processed using a routine known as "plate" (Russ and Russ, 1986) in order to eliminate "noise" or small holes within the parenchyma tissue caused by empty capillaries, without adding to the thickness of the tissue *per se*, Figure 4C. The area (A), perimeter (P), and mean linear intercept (MLI) values were automatically measured using measurement software provided by the analysis system, see Figures 5A-5D. A total of 12-14 fields from four to six different blocks from two rats per time point were so analyzed and tallied.

The number of pores of Kohn was determined by counting the number of fenestrations in the alveolar septal walls within a measurement field, Figure 6. This was done at a higher magnification by changing the microscope's magnification using a combination of higher objective and a 2x optivar. During this procedure, the measured binary image was used as a positioning "map" while counting pores in the live image at the higher magnification to ensure that all counted pores were indeed present within the boundaries of a given measurement field. All fenestrations <20 μm in diameter (Kawakami and Takizawa, 1987) were included in the counts, with the exception of obvious mechanical tears and apparent glancing cuts of an alveolus opening ("mouth") into an alveolar duct. The latter situation can cause what appears to be a normal, as opposed to mechanically torn, looking fenestration, but it is distinguished by the presence of intensely staining elastin that encircles each alveolar mouth. If either side of the fenestration included this characteristic elastin staining, it was not counted as a pore. Both types of artifacts, tearing and glancing cuts of alveolar mouths, were rare and easily recognized.

RESULTS

TiO_2 Clearance Kinetics. The lung burdens of the TiO_2 I and TiO_2-D that were achieved during the 90 day exposure period were ~6.6 and 5.2 mg, respectively. Both types of the TiO_2 were gradually removed from the lungs after cessation of the exposures, although retardations in particle clearance were observed, Figure 7. The retention half time for the TiO_2 I was estimated to be ~171 days, and the retention half

time for the TiO_2-D was much longer, ~500 days. The normal clearance half-time for non-overloading lung burdens of TiO_2-F reportedly ranges between 40 and 100 days (e.g., Ferin and Feldstein, 1978).

Preliminary Tissue Analyses: In the preliminary phase of this study in which lung sections were randomly selected for the A/P and pore number measurements from control samples and lung samples obtained 30, 60, and 90 days after the onset of exposure to the two forms of TiO_2 (F and D), we did not find any major differences among the samples in terms of their A/P ratios, in the numbers of pores relative to parenchyma septal thickness, or in the numbers of pores present when expressed as a function of alveolar perimeter Table 1. However, when we analyzed the day 90 post-TiO_2-D samples that were specifically selected for the presence of foci of AM aggregates, increases in the A/P ratio with corresponding decreases in pore numbers were observed, Table 1 and Figure 8.

In the second phase of this study in which we also biased our sampling to include regions demonstrating focal septal thickening in the 3 and 6 month-post-TiO_2-D samples, we again found evidence that the numbers of pores markedly decreased with increasing septal thickening, as measured by the Area/Perimeter ratio and Mean Linear Intercept value techniques, Figures 9 and 10. The two measurement strategies correlated well with each other, Figure 11, demonstrating that the use of an Area/Perimeter ratio is at least as sensitive for detecting septal thickness changes as the more traditional Mean Linear Intercept method, while offering the additional advantage of being insensitive to tissue anisotropy.

Other Observations: The loss of patent pores of Kohn at sites of alveolar septal thickening were due at least in part to occlusion by Type II cells, Figures 12A and 12B. Shown in Figure 13 is a focal region of AM aggregation observed as of six months after exposure to the TiO_2-D. Sites like these, which show evidence of epithelial cell hyperplasia, and, as previously indicated, a loss in patent pores of Kohn, also appeared to be prominant focal regions where particles became interstitialized. Additionally, ultrastructural evidence of fibrosis was present at these sites, Figure 14.

DISCUSSION

The results from this study of particle overload caused by the deposition of a relatively high lung burden of ultra fine TiO_2 indicate that several anatomical changes occur in the lung during and after the development of such a condition. As early as 60 days after

the onset of exposure to the TiO_2-D, and up to six months after cessation of the aerosol exposure, a focal appearance of aggregates of particle-laden AM in the alveoli was observed, and the alveoli that contained these aggregates of closely apposed AM generally showed evidence of cuboidal cell hyperplasia at the level of light microscopy, which was confirmed to be Type II cell hyperplasia by transmission electron microscopy. The cause for this hyperplastic response obviously requires further investigation, but it would seem reasonable to postulate that the Type II proliferative response may be due to the local over-production of AM-derived pneumocyte growth factor that Brandes and Finkelstein (1989) have shown is released by AM upon activation with a particle stimulus.

Regardless of how it is mediated, an apparent outcome of the Type II cell hyperplastic response and alveolar septal wall thickening is the loss of patent pores of Kohn. As shown herein, such losses are attributable, at least in part, to ingrowths of Type II pneumocytes into the pores. Conceivably, this new observation may lend some further explanation to reductions in AM-mediated lung clearance during particle overload. Although the development and functional roles of the pores of Kohn, which interconnect adjacent alveoli in the same alveolar duct as well as alveoli from different alveolar ducts (Kawakami and Takizawa, 1987), remain poorly understood, they have been postulated for some time now to serve a migratory, interalveolar pathways for the lung's AM. Indeed it is not unusual to find AM with a "squeese through shape" in the pores of Kohn, Figures 15A-15D. Indeed, some investigators have found that virtually all AM are found in alveolar junctional zones where the pores of Kohn frequently occur (Parra et al., 1986). In the context of lung defense against deposited particles, Ferin (1982) has suggested that the alveolar pores increase the efficiency of particle phagocytosis by shortening the distance AM must travel from alveolus to alveolus to reach the particles. With regard to AM-mediated lung clearance *per se*, Green (1973) postulated that AM move by alveolar fluid flows, and that the pores of Kohn may shorten the travel distance between distal alveoli and the terminal airways.

Although we have found an association between diminished particle clearance from the lung and a loss in the pores of Kohn in alveoli, a cause and effect relationship remains to be demonstrated, if, in fact such a relationship exists. As revealed by the work of Mercer and Crapo (1987), rat acini can have as many as 10-12 generations of alveolar ducts. Presently, no information is available as to how the alveoli among the different generations of alveolar ducts might be interconnected via the pores of Kohn in a manner that may favor "short cut" migrations of AM from more distal alveoli to more proximal alveoli, and there is a total lack of information as to what mechanisms may be involved in providing directionality for AM migration via the pores toward the mucociliary apparatus.

Until interalveolar migration of AM is unequivocally demonstrated, even the passage of an AM from one alveolus to a neighboring alveolus on the same alveolar duct via the pores of Kohn will remain a controversial possibility.

Finally, some additional observations made in this investigation are noteworthy. First, we have obtained evidence that extensive interstitialization of particles appears to take place over time in the same alveolar regions where intra-alveolar aggregates of particle-laden AM, Type II cell hyperplasia, and a loss of pores of Kohn occur. Particles that became interstitialized at these sites were well-contained in what appeared to be larger than normal interstitial macrophages (IM) (Sebring and Lehnert, 1992). Moreover, these interstitial sites, which presumably were originally normal alveolar structures, became infiltrated with a variety of cell types, including plasma-like cells and even mast cells (micrographs not shown). It would seem likely that the apparently large fraction of the retained lung burdens that gradually became interstitialized at these sites substantially contributed to the impaired clearance of the ultra-fine TiO_2.

Lastly, as of six months after exposure to the ultra-fine TiO_2, we have observed that fibrosis occurs in close proximity to the interstitial sites where the particles were contained in the IM. This latter observation is consistent with the postulate that particle-laden IM may play an important role in stimulating fibrotic lung responses to particles because of their close proximity to fibroblasts that also reside in the lung's interstitium (Adamson et al., 1989; Adamson et al., 1991).

Acknowledgements: This work was supported by NIH Grants ES04872 and ES01247, and by the U.S. Department of Energy project entitled "Mechanisms of Pulmonary Damage". The structural studies described herein were conducted under the auspices of the U.S. Department of Energy.

REFERENCES

Adamson, IYR, Letourneau, HL, Bowden, DH (1989) Enhanced macrophage-fibroblast interactions in the pulmonary interstitium increases fibrosis after silica injection to monocyte-depleted mice. Amer. J. Pathol. 134:411

Adamson, IYR, Letourneau, HL, Bowden, DH (1991) Comparison of alveolar and interstitial macrophages in fibroblast stimulation after silica and Ion and short asbestos. Lab. Invest. 64:339

Brandes, ME, Finkelstein, JN (1989) Stimulated rabbit alveolar macrophages secrete a growth factor for type II pneumocytes. Am. J. Respir. Cell Mol. Biol. 1:101

Ferin, J (1971) Papain-induced emphysema and the elimination of TiO_2 particulates from lungs. Am. Indus. Hyg. Assoc. J. 32:157

Ferin, J (1982) Pulmonary alveolar pores and alveolar macrophage-mediated particle clearance. Anat. Rec. 203:265

Ferin, J, Feldstein, ML (1978) Pulmonary clearance and hilar lymph node content in rats after particle exposure. Environ. Res. 16:342

Ferin, J, Oberdörster, G., Penney, D.P. (1992) Pulmonary retention of ultrafine and fine particles in rats. Am. J. Respir. Cell Mol. Biol. 6:535

Gibb, FR, Morrow, PE (1962) Alveolar clearance in dogs following inhalation of iron-59 oxide aerosol. J. Appl. Physiol. 17:429

Green, GM (1973) Alveolobronchiolar transport mechanisms. Arch. Intern. Med. 131:109

Kawakami, M, Tekizawa, T (1987) Distributions of pores within alveoli in the human lung. J. Appl. Physiol. 63(5):1866

Lee, KP, Henry, NW, Trochimowicz, HJ (1986) Pulmonary response to impaired lung clearance in rats following excessive TiO_2 dust deposition. Environ. Res. 41:144

Lehnert, BE (1990a) Alveolar macrophages in a particle "overload" condition. J. Aerosol Med. 3(Suppl. 1):S-9

Lehnert, BE (1990b) Lung defense mechanisms against deposited dusts. In Witek, TJ, Schachter, EN (eds), Problems in respiratory care, Vol.3, No.2, J.B. Lippincott Co., Philadelphia, pp.130-162

Lehnert, BE (1992) Pulmonary and thoracic macrophage subpopulations and clearance of particles from the lung. Environ. Health Perspect. 97:17

Lehnert, BE, Morrow, PE (1985) Association of ^{59}iron oxide with alveolar macrophages during alveolar clearance. Exp. Lung Res. 9:1

Lehnert, BE, Valdez, YE, Sebring, RJ, et al. (1990) Airway intra-luminal macrophages: Evidence of origin and comparisons to alveolar macrophages. Am. J. Respir. Cell Mol. Biol. 3:377

Mercer, RR, Crapo, JD (1987) Three-dimensional reconstruction of the rat acinus. J. Appl. Physiol. 63(2):785

Morrow, PE (1988) Possible mechanisms to explain dust overloading of the lungs. Fund. Appl. Toxicol. 10:197

Oberdörster, G, Ferin, J, Morrow, PE Volumetric loading of alveolar macrophages (AM): A possible basis for diminished AM-mediated particle clearance. Exp. Lung Res. 18:87

Parra, SC, Burnette, R, Price, HP, et al. (1986) Zonal distribution of alveolar macrophages, type II pneumocytes, and alveolar septal connective tissue gaps in adult human lungs. Am. Rev. Respir. Dis. 133:908

Russ, JC, Russ, JC, Jr. (1984) Image processing in a general purpose microcomputer. J. Micros. 135:89

Russ, JC, Russ, JC,JR. (1986) Automatic editing of binary images for feature isolation and measurement. Microbeam Analysis :505

Sebring, RJ, Lehnert, BE (1992) Morphometric comparisons of rat alveolar macrophages, pulmonary interstitial macrophages, and blood monocytes. Exp. Lung Res. 18:479

Snipes, MB, Clem, MF (1981) Retention of microspheres in rat lung after intratracheal instillation. Environ. Res. 24:33

Wolff, RK, Henderson, RF, Snipes, MB et al. (1987) Alterations in particle accumulation and clearance in lungs of rats chronically exposed to diesel exhaust. Fund. Appl. Toxicol. 9:154

FIGURE LEGENDS

Figures 1A and 1B: TEM of aggregates of particle-laden AM (AM) and cuboidal cell (Type II cell) hyperplasia (II) were evident in the TiO_2-D lungs as early as 60 days after the onset of exposure.

Figure 2: The aggregates of particle-laden AM (*) were focal in nature. This light micrograph was taken from a lung that had been exposed to the TiO_2-D for 60 days.

Figures 3A-3C: (A) The live image from a light microscope of a lung field was digitized to a 64 gray-level image. (B) A gray-level histogram of the image was generated, (C) and gray-level thresholding was used to create a binary image of the gray-level image.

Figures 4A-4C: (A) At higher magnification, non-parenchymal features were recognized and edited from the lower magnification binary image, e.g., alveolar macrophages. The black circled regions demonstrate what would have been removed from the corresponding image in 3C giving an edited image (B) of the fine parenchymal structure. "Holes" in the binary image (B) due to structures such as empty or partially filled capillaries were minimized (C) using a computer "plate" technique.

Figures 5A-5D: (A) The parenchyma area (white regions) in the binary image was measured and expressed in μM^2. (B) The perimeter lengths of the alveolar surfaces in the field were collectively measured in μM. Data from (A) and (B) were used to determine the A/P ratio that served as an index of alveolar septal thickening. (C) and (D) represent only 28 of the 256 image lines that intercept the parenchyma. All the line segment lengths resulting from the interception of all 256 lines are averaged and reported as the Mean Linear Intercept value expressed in μM

Figure 6: Light Micrograph of a lung section showing the appearance of two fenestrations (P: pores of Kohn) that are present in 3 adjacent alveoli (ALV).

Figure 7: The accumulation of TiO_2 F (closed circles) and TiO_2 D (open circles) during the 90 day exposure period, and the retention of the two types of TiO_2 over a one year post exposure period.

Figure 8: Comparisons of the A/P ratios and pore numbers measured from the 90 day control samples and the 90 day TiO_2-D samples. Sampling was biased for the occurrence of focal aggregates of particle-laden AM in the TiO_2-D samples. Each point represents parenchyma within a 385 x 290 μM measurement field. Sampling of TiO_2-D did not include "normal" looking adjacent parenchyma within the same section.

Figure 9: A/P ratio values and pore numbers measured with the three and six month control and TiO_2-D samples. The TiO_2-D samples were selected for the appearance of aggregates of particle-containing AM. Each point represents parenchyma within a 617 x 465 μM measurement field. Sampling of TiO_2-D included both focal aggregates as well as "normal" looking adjacent parenchyma within the same section.

Figure 10: MLI values and pore numbers measured with the three and six month control and TiO_2-D samples. The TiO_2-D samples were selected for the appearance of aggregates of particle-containing AM. This data is from the identical measurement fields as in Figure 9.

Figure 11: Correlation of the A/P ratio and MLI values obtained from the control and TiO_2-D exposed three and six month samples. Both parameters evidently serve equally well in depicting structural changes that occur in regions containing aggregates of particle-laden AM, i.e., alveolar septal thickening.

Figures 12A and 12 B: Electron micrographs showing the occlusion of the pores of Kohn (open arrows) by Type II pneumocytes (II). A common ultrastructural feature of the pores of Kohn is the presence of collagen around their openings (closed arrows).

Figure 13: A focal region of AM aggregation (AM) observed as of six months after exposure to the TiO_2-D. Particles in this region are extensively interstitialized. Virtually all of the interstitialized particles (I) appear to be well contained in interstitial macrophages. Arrows point to Type II cell hyperplasia. *: a particle containing interstitial macrophage that is located in the perivascular space.

Figure 14: A region of interstitialized particles (contained in an interstitial macrophage, IM) where an abnormal abundance of collagen (C) is found. ALV: alveolus; II: Type II pneumocyte.

Figures 15A-15D: AM as well as polymorphonuclear leukocytes (when present in elevated numbers) can be frequently observed to be in the pores of Kohn. AM: alveolar macrophages; PMN: polymorphonuclear leukocyte; II: a Type II cell that has co-localized with a pore; arrows: pores of Kohn.

Table 1: Area, Perimeter, and Pore Number Data Obtained from Control, and TiO_2-F and TiO_2-D Exposed Lungs on Days 30, 60, and 90.

	Total Perimeter (μm)	Total Area (μm^2)	Area/ Perimeter	# Pores	Perimeter (μm)/ Pore
Control 30	39,605	165,016	4.17	24	1650/pore
Control 60	42,299	158,564	3.75	20	2115/pore
Control 90	38,574	129,232	3.35	25	1543/pore
Control Total	120,478	452,812	3.75	69	1746/pore
TiO_2F 30	42,643	158,942	3.73	23	1854/pore
TiO_2F 60	42,529	144,004	3.38	22	1933/pore
TiO_2F 90	45,708	159,079	3.48	25	1828/pore
TiO_2D 30	44,286	165,980	3.75	20	2214/pore
TiO_2D 60	43,227	166,297	3.85	22	1965/pore
TiO_2D 90	60,250	246,268	4.09	38	1586/pore
TiO_2D 90(*)	38,721	197,536	5.10	7	5532/pore

* Selected for regions of activity

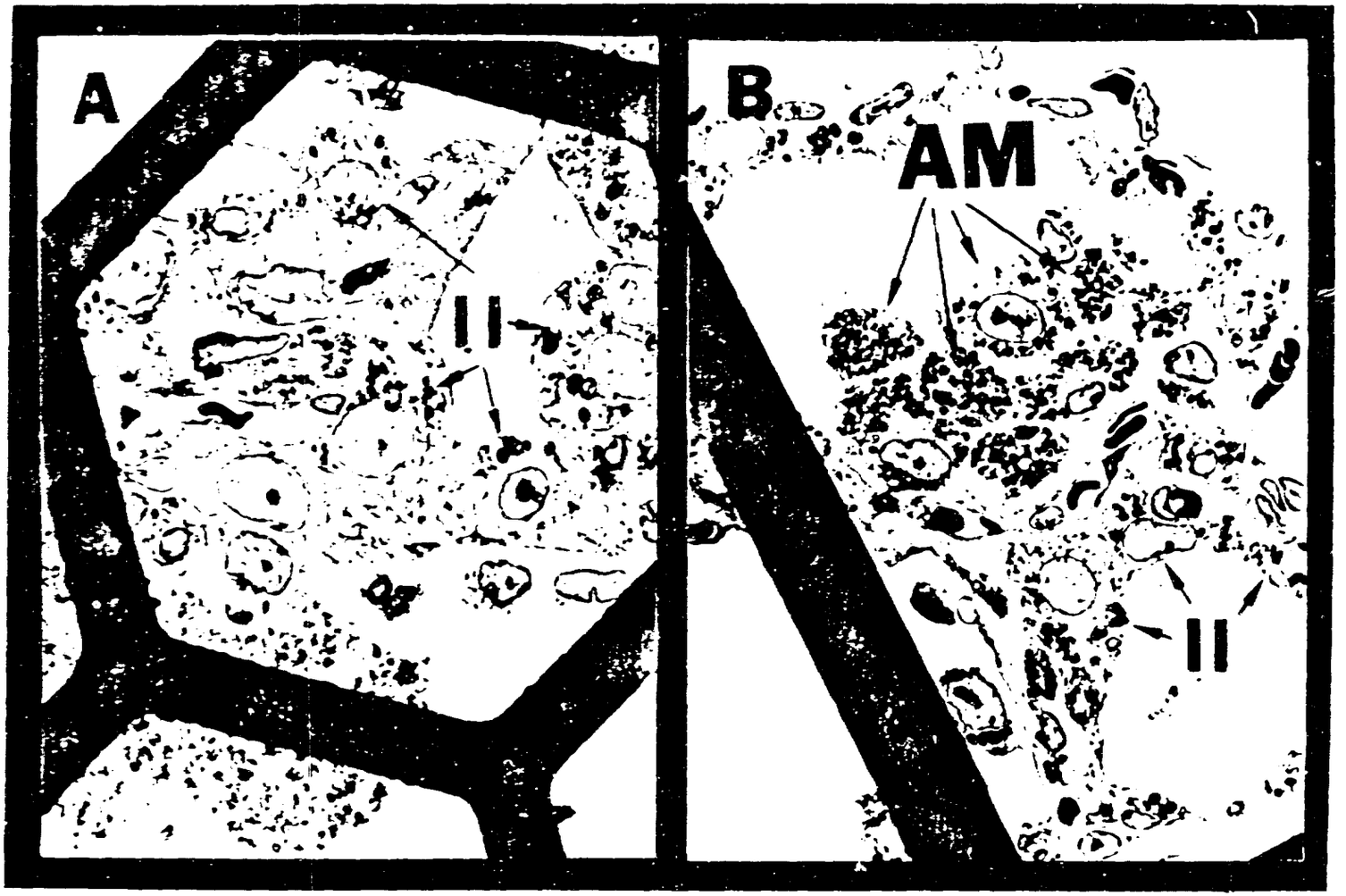
A
II
B
AM
II

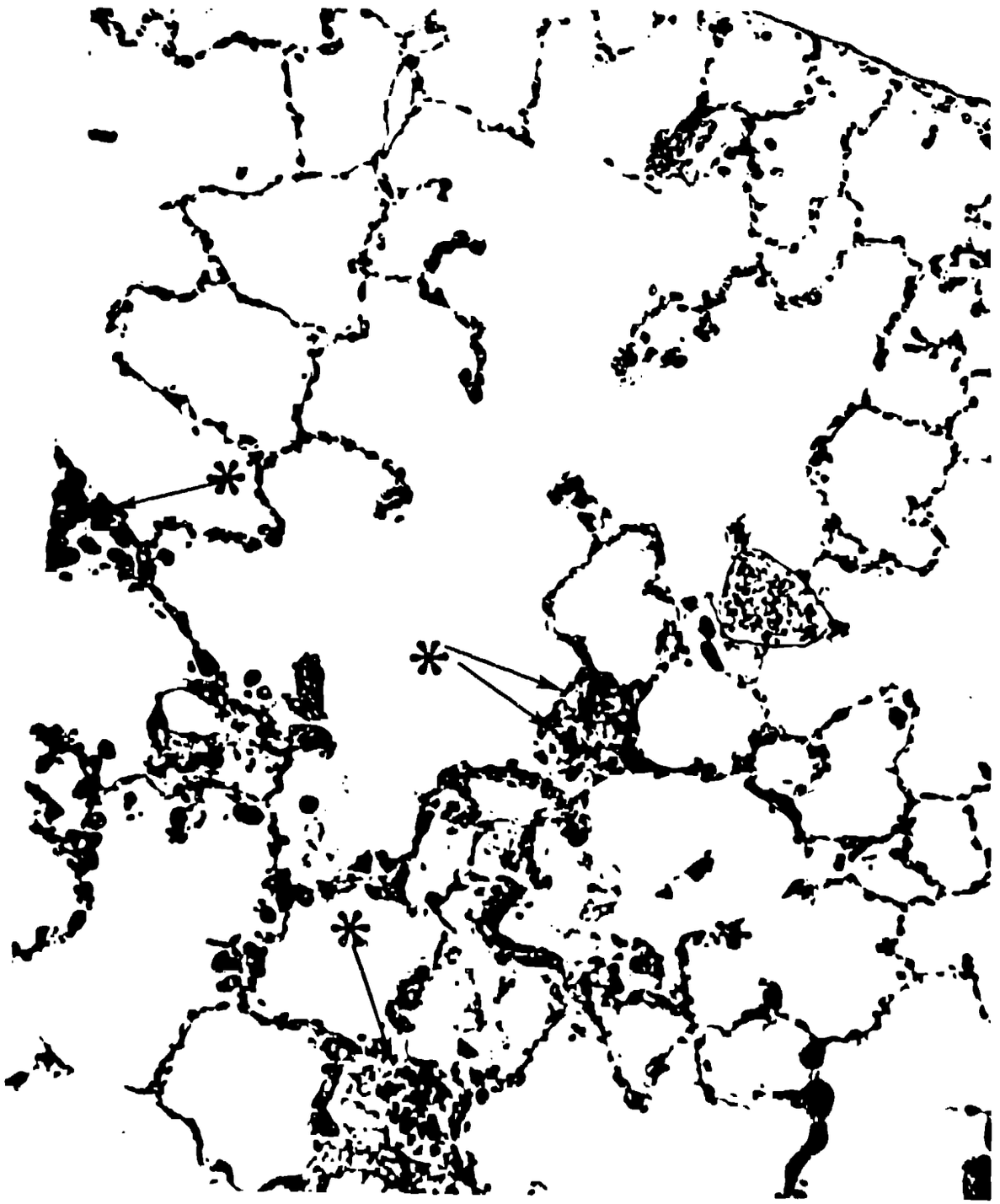

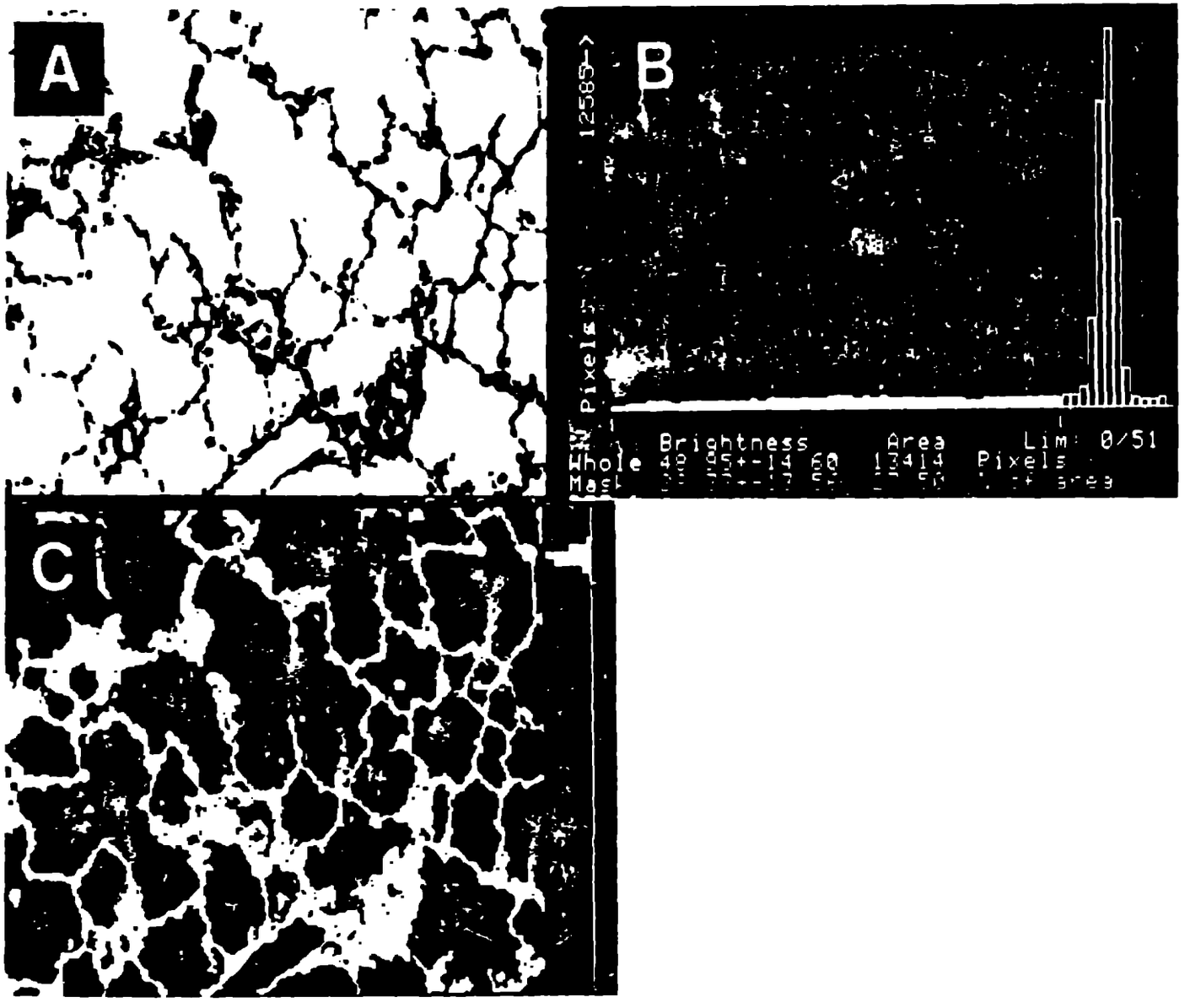
A
B
C
Brightness
Area
Pixels

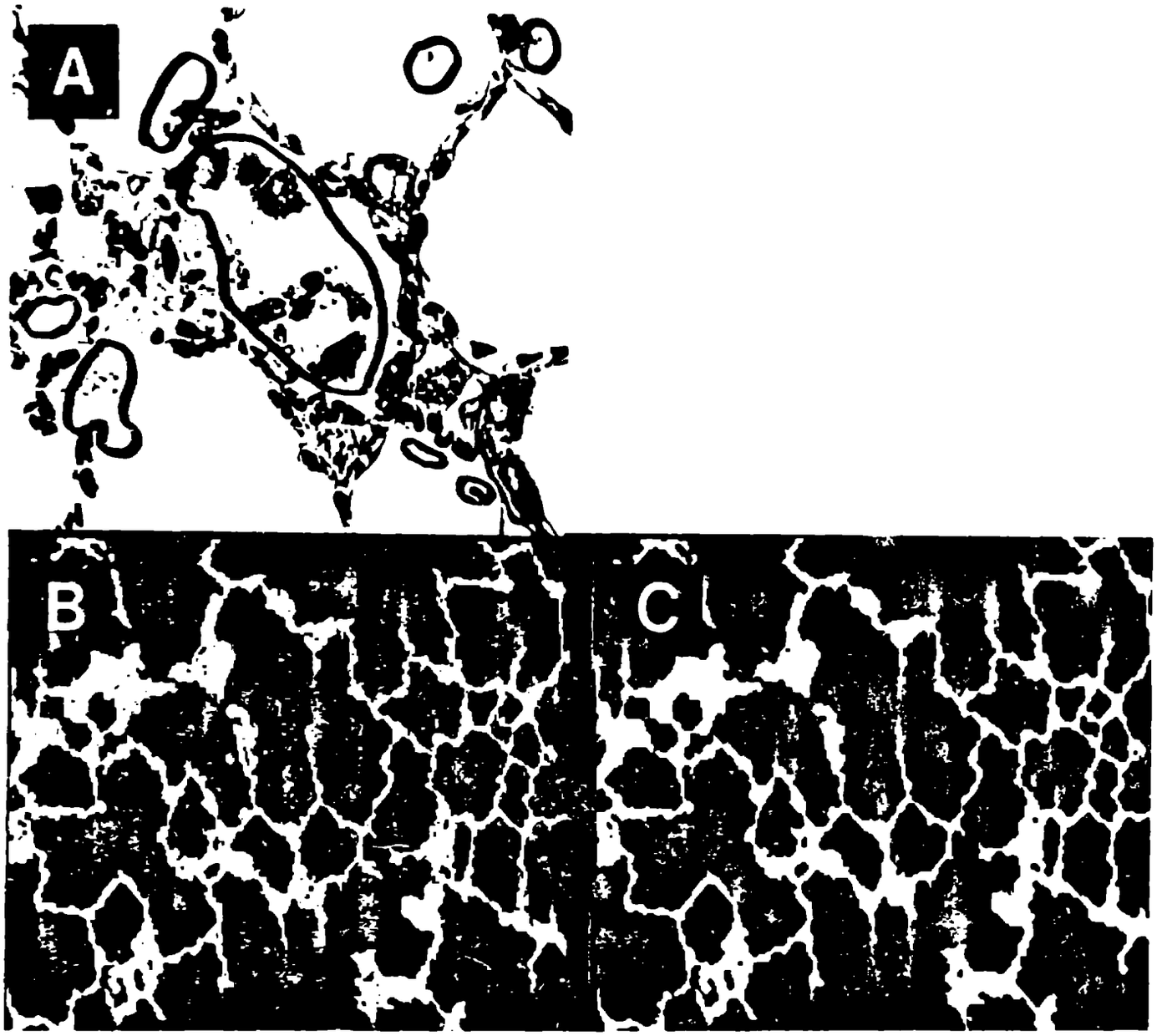
A
B
C

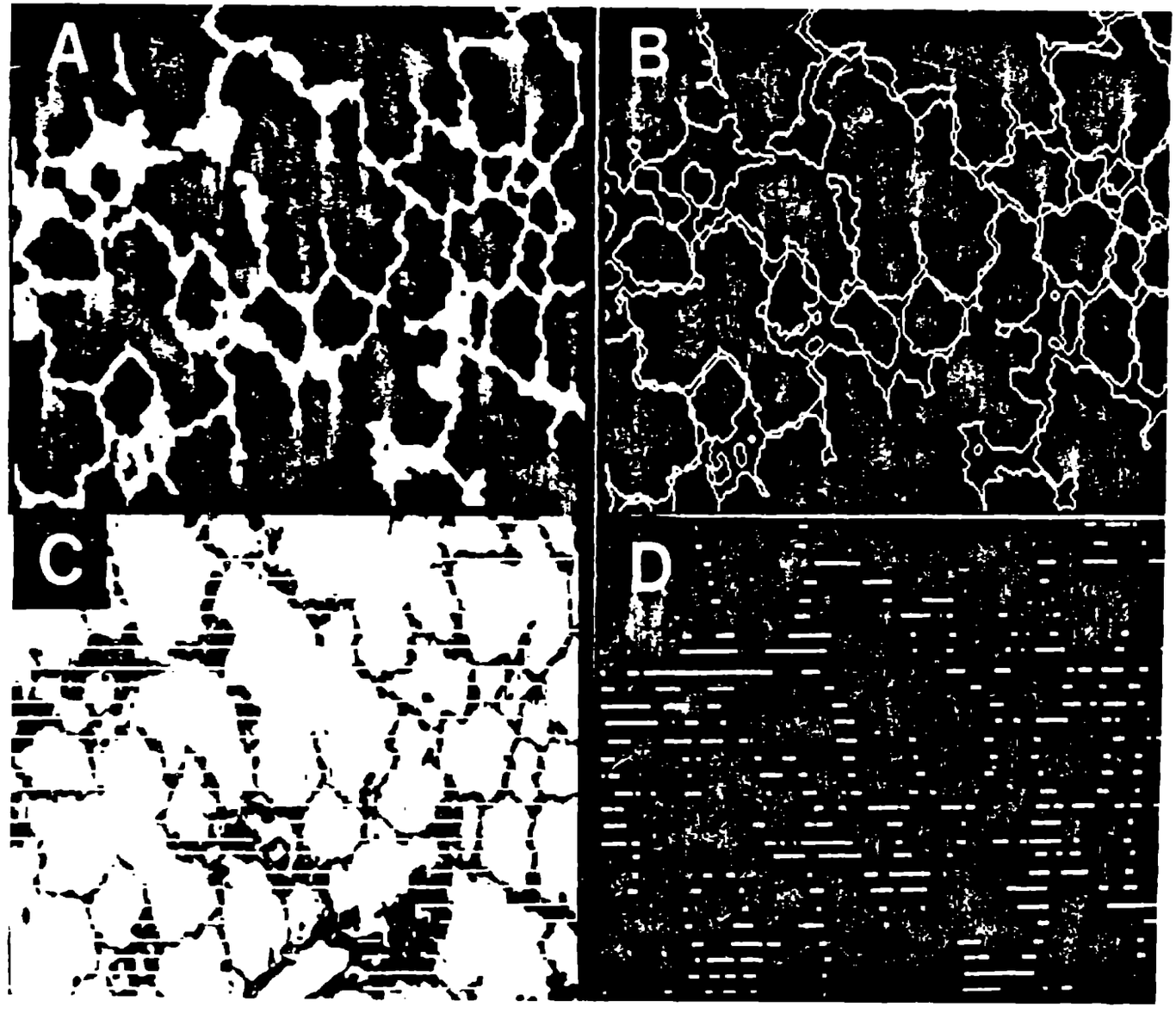
A
B
C
D

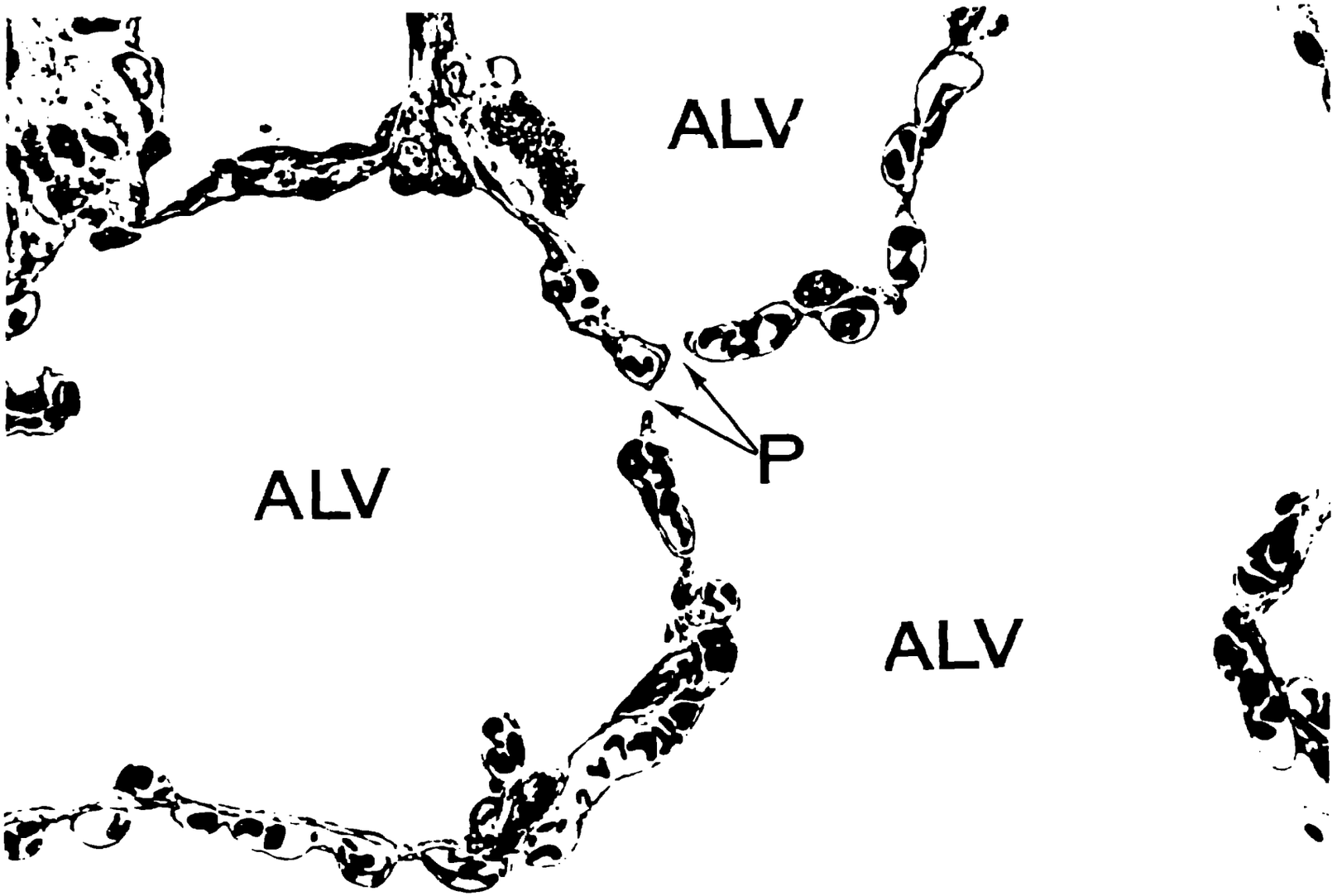
ALV
P
ALV
ALV

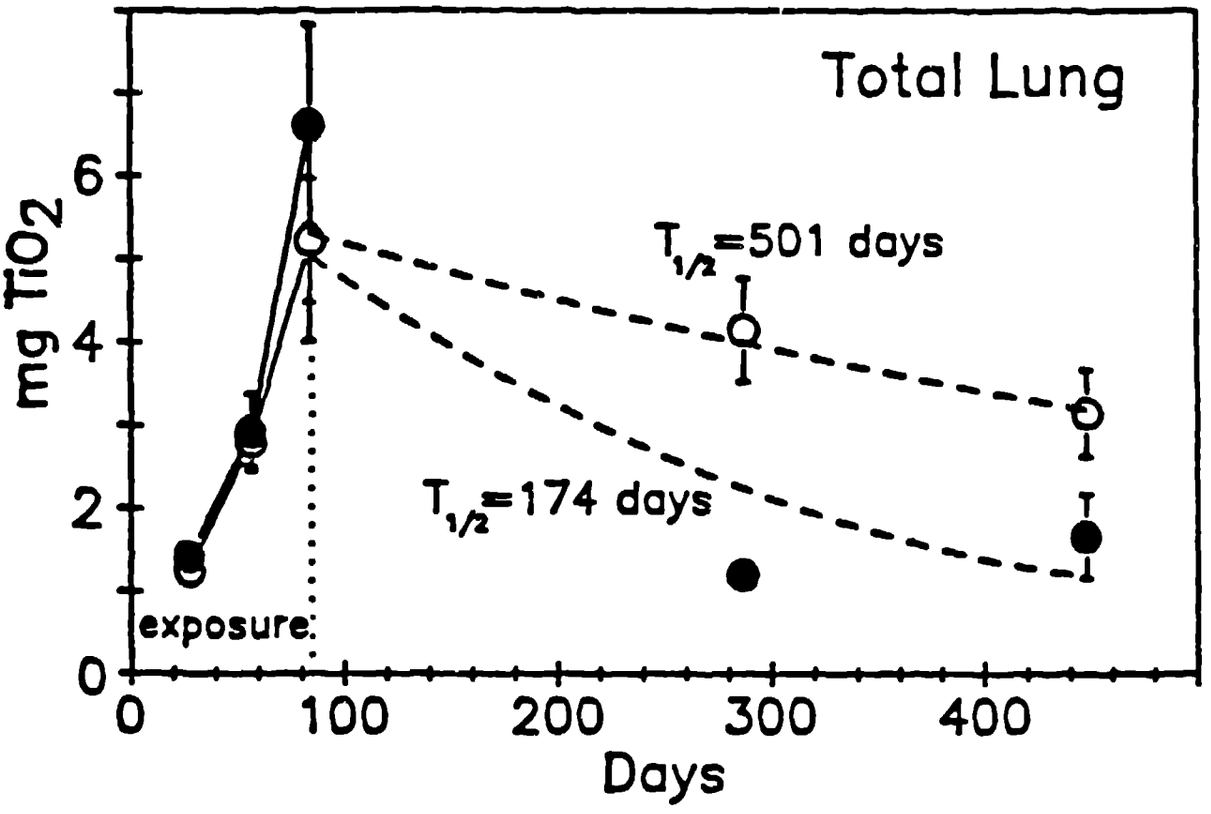
Total Lung
mg TiO2
6
4
2
0
$T_{1/2}$=501 days
$T_{1/2}$=174 days
exposure
0
100
200
300
400
Days

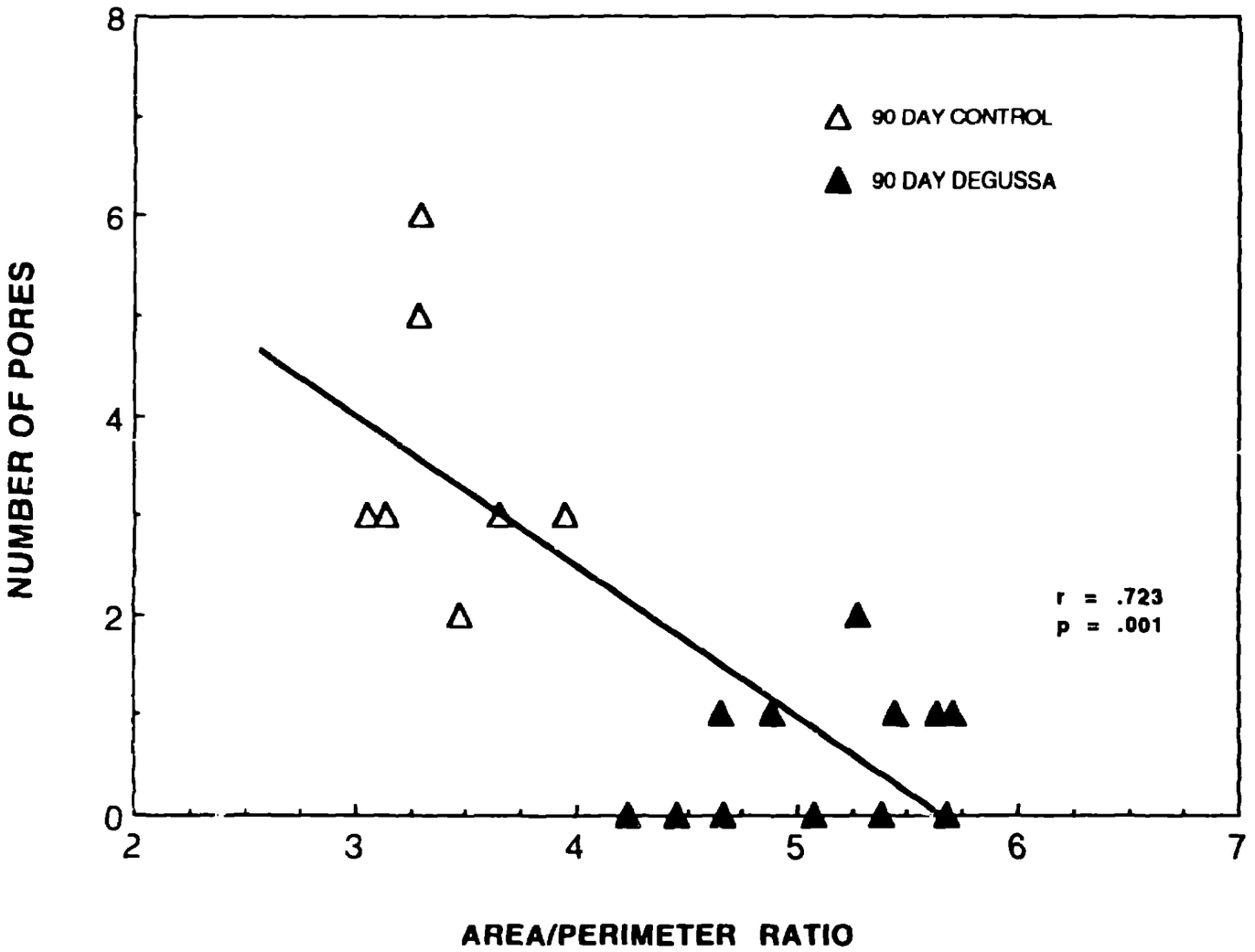
90 DAY CONTROL
90 DAY DEGUSSA
r = .723
p = .001
NUMBER OF PORES
AREA/PERIMETER RATIO
0
2
4
6
8
2
3
4
5
6
7

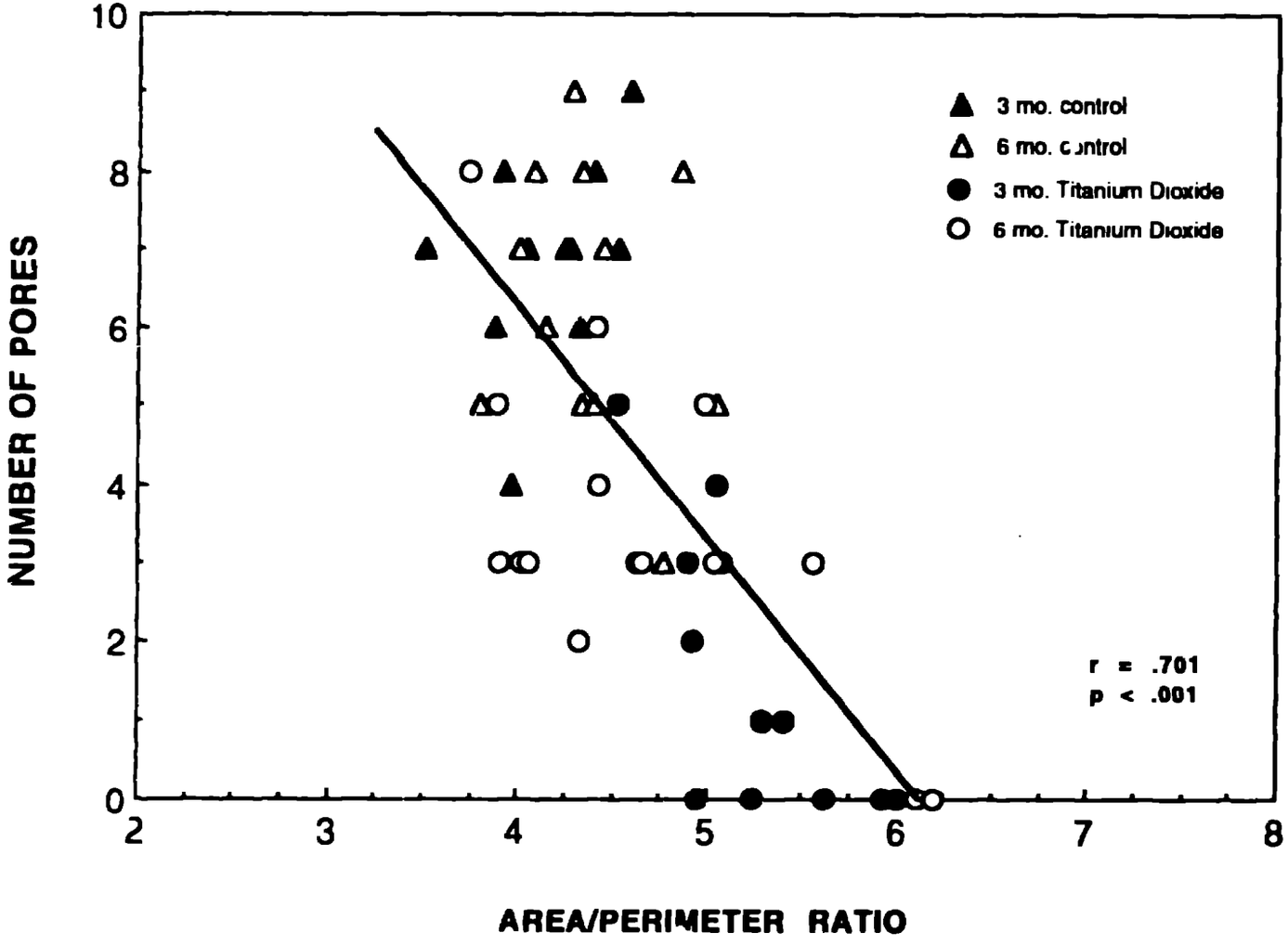
NUMBER OF PORES
AREA/PERIMETER RATIO
3 mo. control
6 mo. control
3 mo. Titanium Dioxide
6 mo. Titanium Dioxide
r = .701
p < .001
0
2
4
6
8
10
2
3
4
5
6
7
8

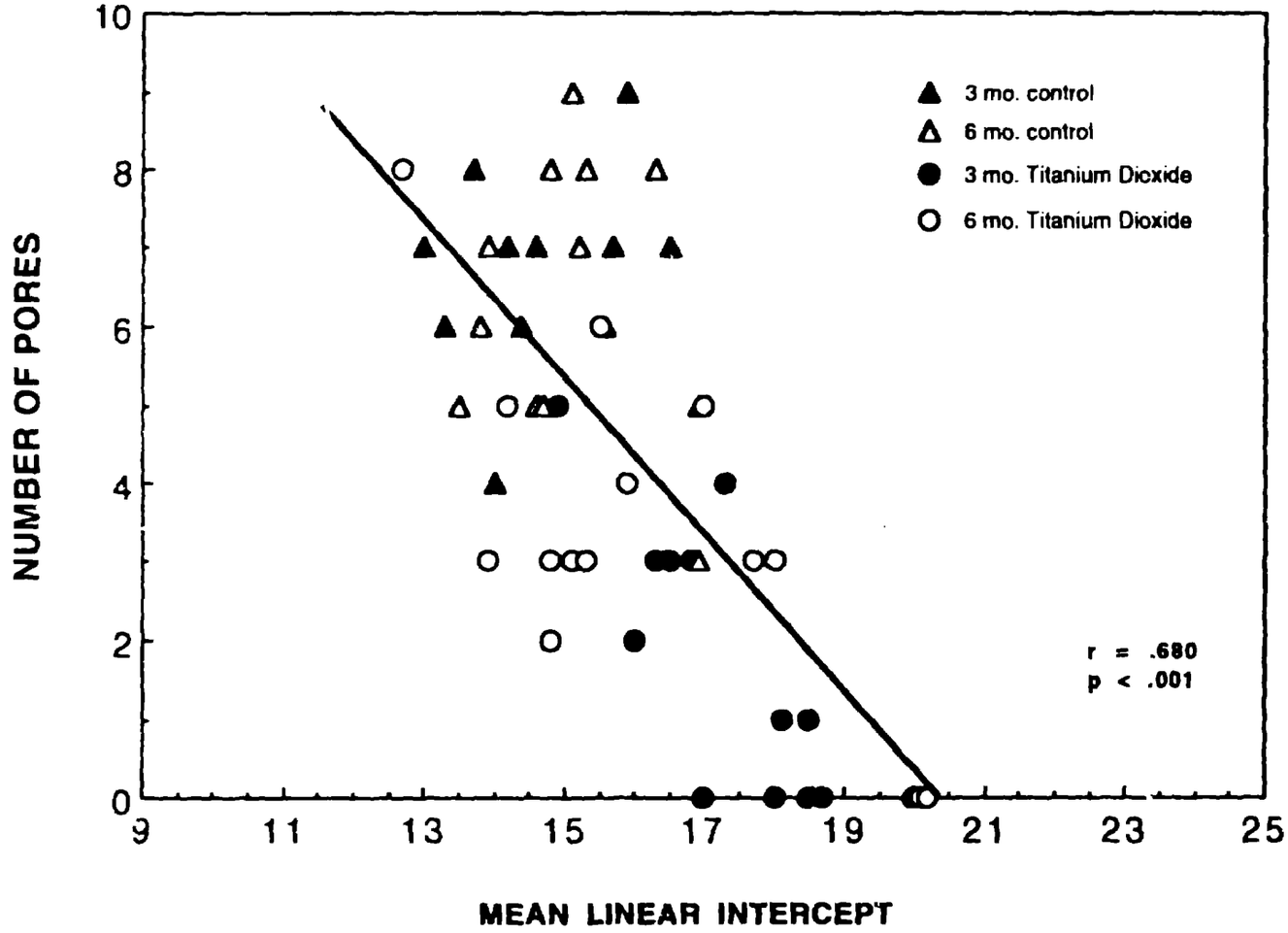
10
8
6
4
2
0
9
11
13
15
17
19
21
23
25
NUMBER OF PORES
MEAN LINEAR INTERCEPT
3 mo. control
6 mo. control
3 mo. Titanium Dioxide
6 mo. Titanium Dioxide
r = .680
p < .001

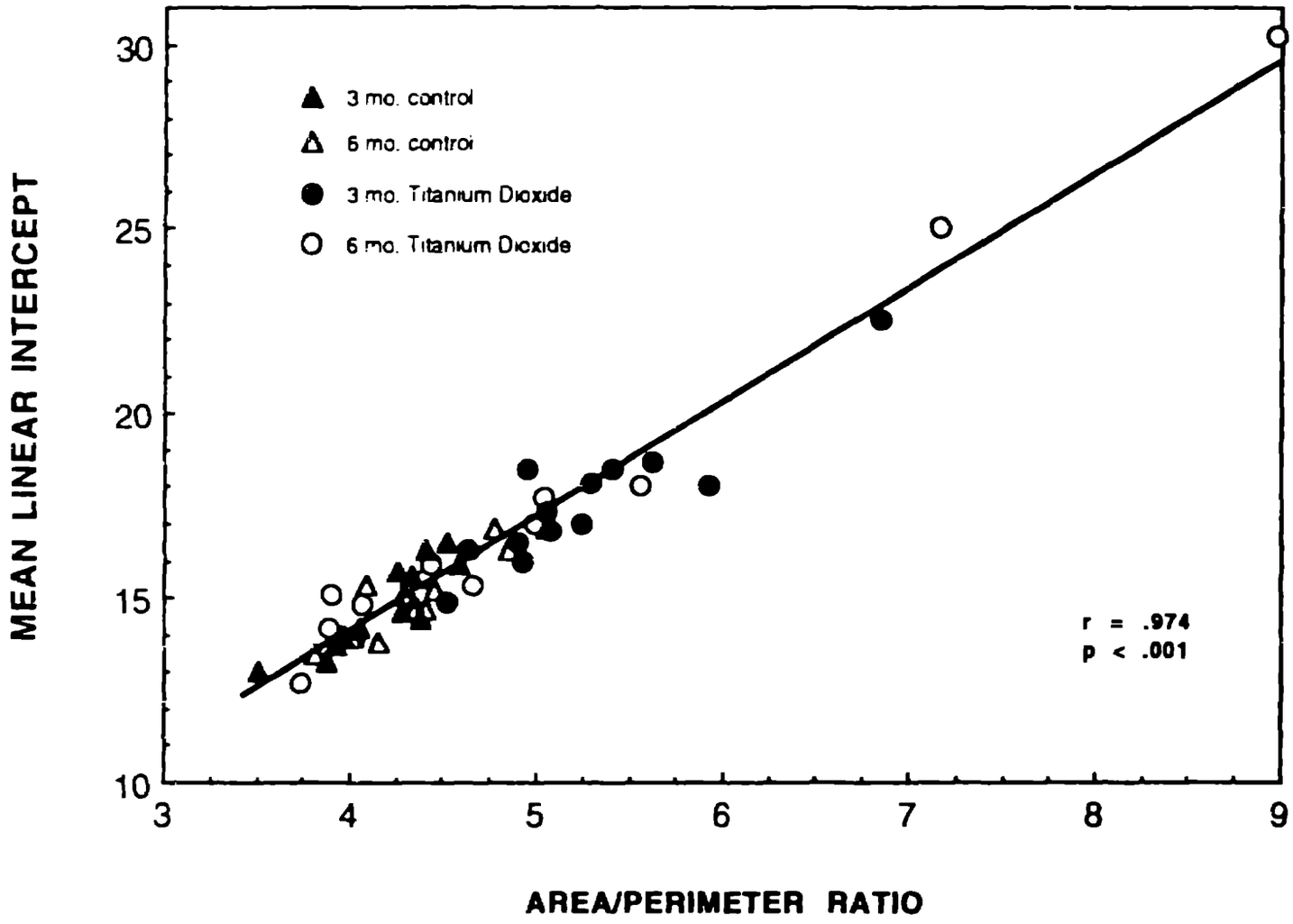
MEAN LINEAR INTERCEPT
30
25
20
15
10
3
4
5
6
7
8
9
AREA/PERIMETER RATIO
3 mo. control
6 mo. control
3 mo. Titanium Dioxide
6 mo. Titanium Dioxide
r = .974
p < .001

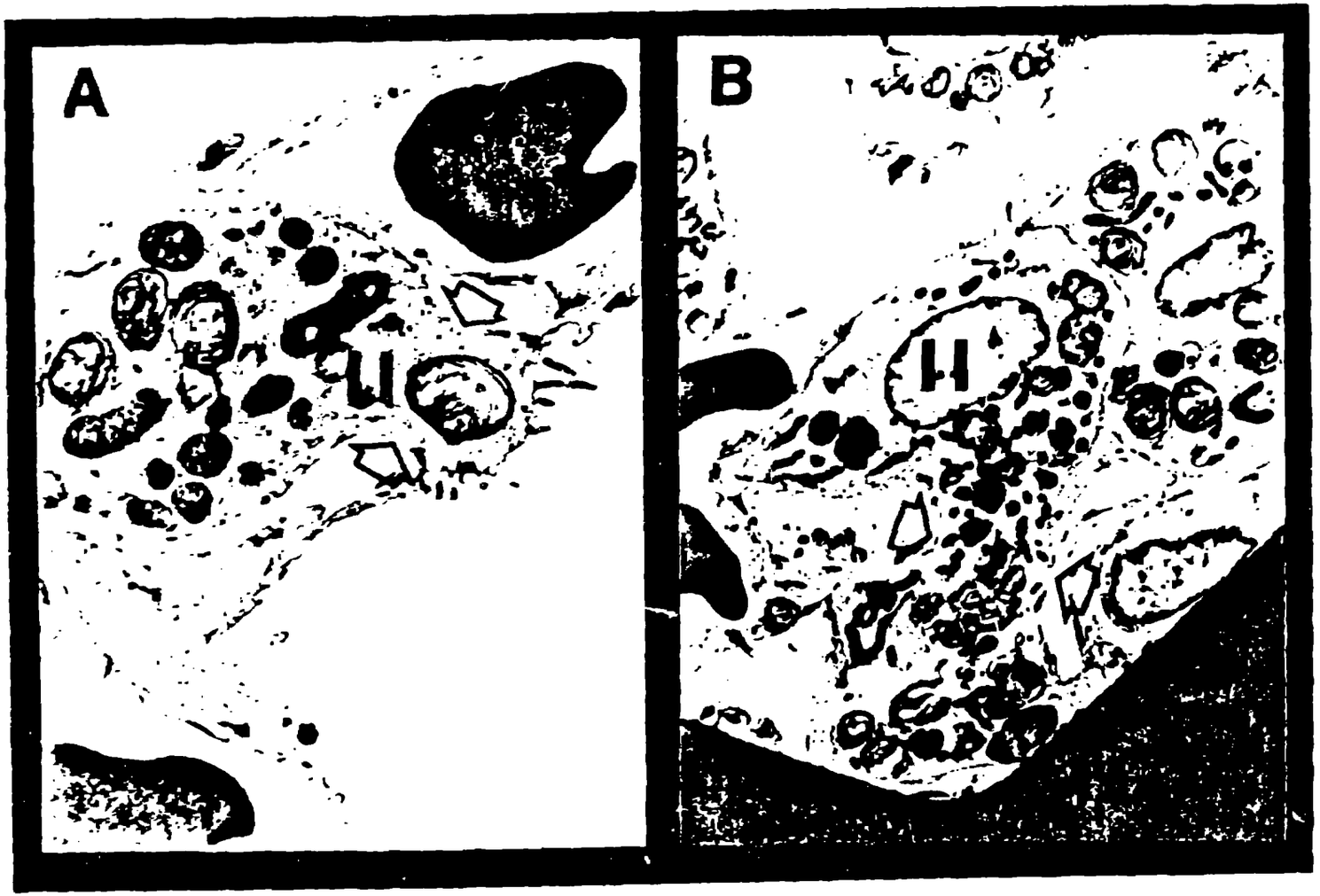
A
B
H

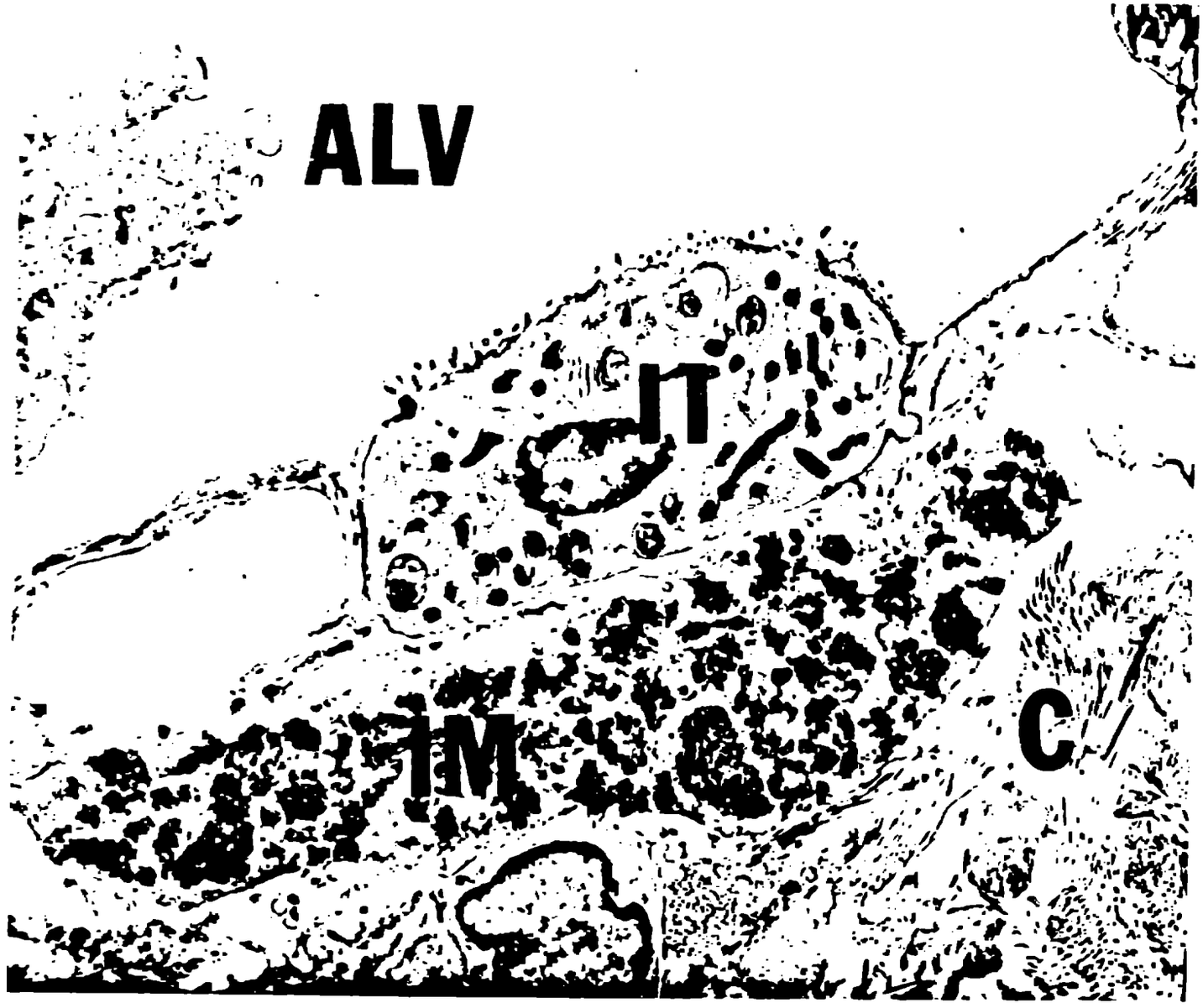
ALV
IT
M
C

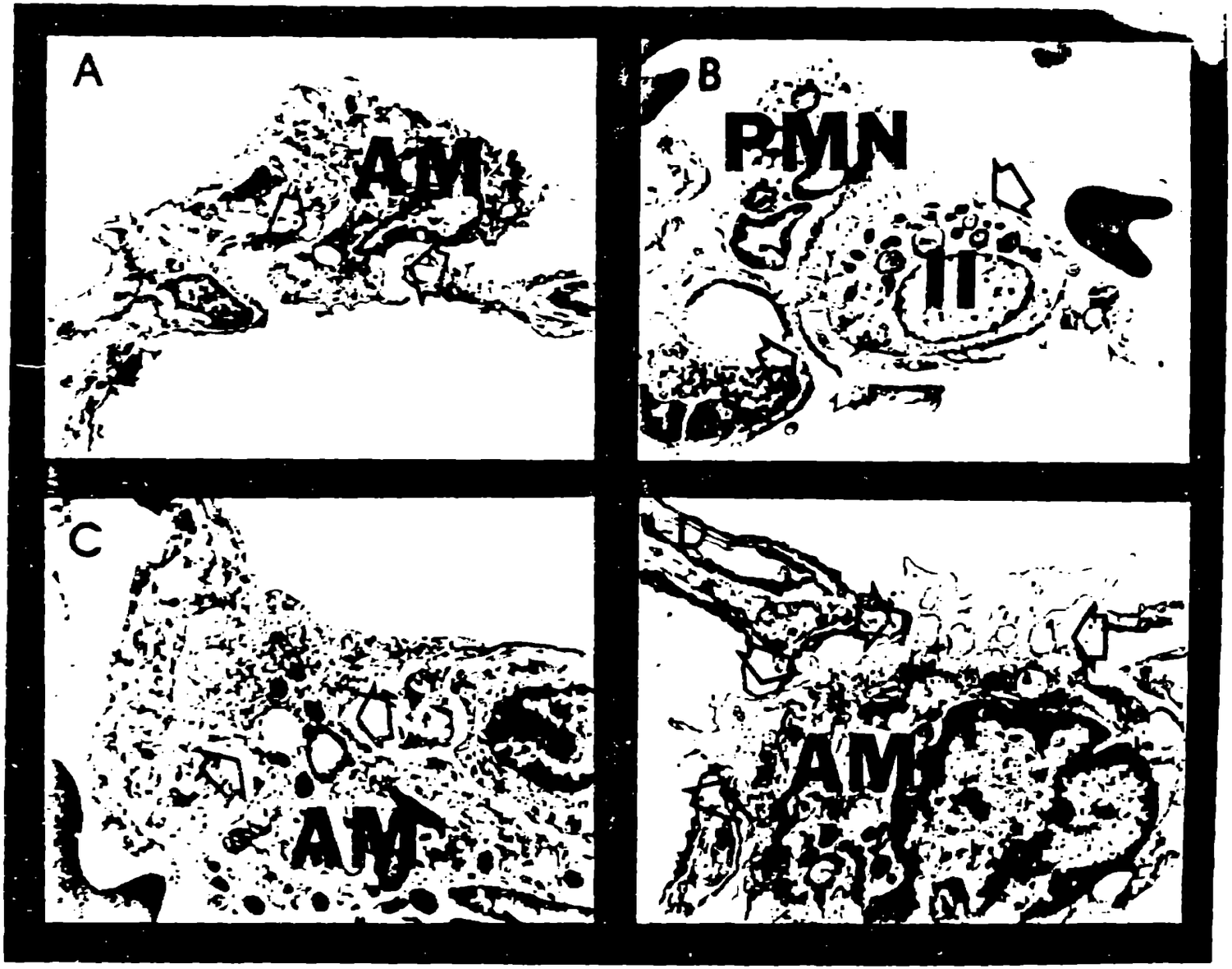
A
AM
B
PMN
II
C
AM
D
AM